THE JOURNAL OF PHYSICAL CHEMISTRY Letters

Letter

Cite This: J. Phys. Chem. Lett. 2019, 10, 40−47

pubs.acs.org/JPCL

Superconductivity and Phase Stability of Potassium-Intercalated *p*-Quaterphenyl

Jia-Feng Yan,[†,∥] Guo-Hua Zhong,[‡,∥] Ren-Shu Wang,[†,¶] Kai Zhang,[†] Hai-Qing Lin,[*,§] and Xiao-Jia Chen[*,†]

[†]Center for High Pressure Science and Technology Advanced Research, Shanghai 201203, China

[‡]Shenzhen Institutes of Advanced Technology, Chinese Academy of Sciences, Shenzhen 518055, China

[¶]School of Materials Science and Engineering, Hubei University, Wuhan 430062, China

[§]Beijing Computational Science Research Center, Beijing 100193, China

Supporting Information

ABSTRACT: To explore more novel superconductors, we have synthesized the potassium-doped *p*-quaterphenyl by an annealing or just a pestling process. The Meissner effect with critical temperatures ranging from 3.5 to 120 K is found by the magnetic susceptibility measurements in doped samples. The primary superconducting phase with a critical temperature of 7.2 K can be duplicated in the annealed and pestled samples. The charge transfer from metal to molecule is confirmed from the Raman scattering measurements. The X-ray diffraction analysis suggests that the low-temperature superconducting phase is due to the two-electron doping, whereas the high-temperature one corresponds to the high doping content. The occurrence of superconductivity in potassium-doped *p*-quaterphenyl supports the chain link organic molecules as promising candidates for high-temperature superconductors. This work also provides a simple method for synthesizing organic superconductors by pestling without annealing.

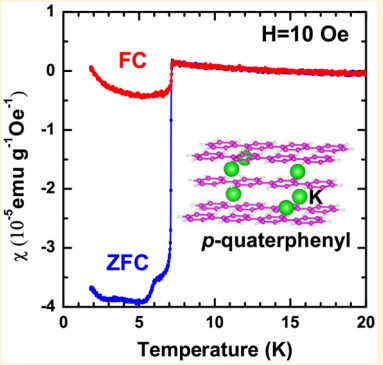

The perpetual enthusiasm of chasing novel high-temperature superconductors is never dampened. Organic compounds are predicted as candidates of superconductors with high critical temperature (T_c) even above room temperature.[1,2] Poly(*para*-phenylenes) (PPPs), as an important component of quasi-one-dimensional conducting polymers,[3] have a great potential to be superconductors because of the great features of high conductivity,[4] the absence of isomerization upon doping, nondegenerate ground-state structure, large Coulomb correlation,[5] and bipolaron conducting mechanism.[6] *p*-Oligophenyls with a shorter chain possess a molecular structure similar to that of PPP, with infinite benzene rings linked by a single C−C bond in the *para* position. In fact, PPP also exhibits high electrical conductivity upon doping of donors or acceptors.[7] The conductivity of doped PPP significantly increases with the increasing chain length,[8] in contrast to the band gap's decrease as a function of increasing quinoid character of the backbone.[9]

Recently, potassium (K)-doped *p*-terphenyl, as a member of *p*-oligophenyls, has attracted a lot of attention because of the discovery of superconductivity with critical temperatures of 7.2, 43, and even 123 K.[10−12] These discoveries support previous predictions[13] based on calculations, which claim that K-doped solid benzene shows spuerconductivity with the most stable phase of T_c around 6.2 K, and this superconducting phase shares the common feature of aromatic hydrocarbon superconductors. By comparison of the first-principles calculations and the experimentally observed X-ray diffraction (XRD) patterns,[14] the superconducting phase with T_c of 7.2 K[10] in K-doped *p*-terphenyl should be a mixture phase with a doping level in the range of 2−3. The 7.2 K superconducting phase reemerges in K-doped biphenyl,[15] *p*-quinquephenyl,[16] 2,2′-bipyridine,[17] and triphenylbismuth.[18] Subsequently, a new report[19] provided the spectroscopic evidence for superconducting pairing gaps persisting to 120 K or above on the surface-doped *p*-terphenyl single crystals by measurements of angle-resolved photoemission spectroscopy. The gapped phases were also observed in K-doped single-layer *p*-terphenyl films grown on Au(111).[20] The unresponsive feature of this gap to the applied magnetic field up to 11 T implies the extremely high upper critical field for such high T_c superconductors. Afterward, another superconducting phase with high T_c of 107 K was reported in *p*-terphenyl flakes upon doping potassium.[21] The discussion about band structure and density of states of *p*-terphenyl helps in the search for high T_c superconductors with electronic structure similar to that of *p*-terphenyl.[14,22,23] A proposal of the mechanism driving the remarkable superconducting transition in K-doped *p*-terphenyl is the Fano resonance between superconducting gaps near a Lifshitz transition.[24] Meanwhile, a superconductivity-like

Received: October 26, 2018
Accepted: November 24, 2018
Published: November 25, 2018

DOI: 10.1021/acs.jpclett.8b03263
J. Phys. Chem. Lett. 2019, 10, 40−47

transition was observed in K-doped *p*-terphenyl and *p*-quaterphenyl by high-pressure synthesis.[25] The observations of ferromagnetic background and the absence of diamagnetic magnetic susceptibility have led to claims that it is insufficient to regard K-doped *p*-terphenyl and *p*-quaterphenyl as superconductors. Superconductivity in K-doped *p*-terphenyl gets support from both experimental[10−12,19−21] and theoretical[14,22,24] works. Thus, the possibility of superconductivity in *p*-quaterphenyl, which consists of one more benzene ring than *p*-terphenyl, is worthy of further exploration.

p-Quaterphrnyl, $C_{24}H_{18}$, as a member of conjugated semiconducting oligomers, has extensive potential for use in organic thin-film transistors,[26] organic light-emitting diodes,[27] and organic lasers[28] because of the optical activation.[29] After the applications in photoelectricity, the high possibility of superconductivity in $C_{24}H_{18}$ will enrich other applications. In this work, we report the finding of superconductivity in K-doped *p*-quaterphenyl ($K_xC_{24}H_{18}$) fabricated by an annealing or a pestling process. The magnetization measurements provide solid evidence of the presence of Meissner effect with T_c's ranging from 3.5 to 120 K. The primary 7.2 K superconducting phase can be duplicated in both the annealed and pestled samples. Another weak superconducting phase with a high T_c of 120 K is observed in the pestled sample as well. The Raman scattering measurements provide the evidence of the formation of bipolarons. The chemical structures of superconducting phases are predicted by the random structure search. The electronic properties of different structures indicate that the low-T_c phase of 7.2 K comes from the two-electron doping while the high-T_c superconductivity of 120 K is possibly driven by the higher doping concentration. The realization of superconductivity in $K_xC_{24}H_{18}$ adds a new league of superconductors in the *p*-oligophenyl family. In addition, this work also provides a simple method to synthesize the organic superconductors by pestling without annealing.

The $K_xC_{24}H_{18}$ samples were synthesized in diverse conditions. One process is that the samples are fabricated by annealing after heating the mixtures of $C_{24}H_{18}$ and K metal, called annealed samples, which is similar to the process of previous studies.[10,15−17] Another method is that the samples are obtained by pestling the mixtures without annealing, termed pestled samples. (Details can be found in the Supporting Information.) The paramagnetic behavior in the samples without superconductivity fits well with the Curie−Weiss law. Nevertheless, several samples, listed in Table 1, exhibit superconductivity. The primary superconducting phase with critical temperature of 7.2 K is repeated in sample nos. 7, 16, 27, 43, and 50. The additional 4.3 and 6.1 K superconducting phases accompany the primary superconducting phase, respectively. Moreover, the superconductivity of 7.2 K was obtained in the pestled sample no. 50. Interestingly, another weak superconducting phase with a high T_c of 120 K was observed in the pestled sample no. 10.

Table 1. Summary of $K_xC_{24}H_{18}$ Samples with Different Superconducting Transition Temperatures (T_c) Synthesized at Various Conditions of Annealing Temperature (T_{an}) and Time

no.	ratio	T_{an} (K)	time (days)	T_c (K)	shielding fraction (%)
7	3	605	10	4.3, 7.2	0.00927
16	3	605	10	6.1, 7.2	0.1488
27	3	605	10	7.2	0.00528
43	4	623	3	7.2	0.00256
52	4	615	3	3.5	trace
50	4	pestle	none	7.2	0.0116
10	3	pestle	none	120	0.00688

The superconductivity of $K_xC_{24}H_{18}$ was characterized by magnetization measurements. Figure 1a displays the temperature dependence of the magnetic susceptibility χ in a low magnetic field of 10 Oe with the field-cooling (FC) and zero-field-cooling (ZFC) runs for sample no. 16. The ZFC curve shows a sharp drop at the temperature of 7.2 K with a second drop at the temperature of 6.1 K, while a platform after the drop at the temperature of 7.2 K can be observed in the FC run. The magnetic measurements of this sample reveal two superconducting phases with T_c of 6.1 and 7.2 K, respectively. Supposing that the density δ of this sample is about 3 g/cm^3, we get the shielding fraction $4\pi\chi\delta$ = 0.1488% from Figure 1a. The volume fraction of the superconducting content is not very high because of the presence of impurities. The obtained superconductivity of $K_xC_{24}H_{18}$ was further demonstrated by the shift of the temperature−χ curve by the applied magnetic fields. In Figure 1b, the T_c gradually diminishes with increasing magnetic field because the superconducting fraction is suppressed by the applied magnetic field. The second 6.1 K superconducting phase is hardly observed at the magnetic field larger than 400 Oe, while the 7.1 K superconducting phase remains until 1000 Oe.

The Meissner effect of this superconductor was further demonstrated by magnetization measurements. Figure 1c,d presents the magnetization hysteresis loop up to 1000 Oe at various temperatures from 1.8 to 7 K in the superconducting state, after removal of the paramagnetic background (a straight line). In Figure 1c, the lower critical magnetic field H_{c1} is determined by the deviation from linearity in M versus H curves. The linearity region increases with decreasing temperature; meanwhile, the H_{c1} becomes higher along with lower temperature. Figure 1d represents the magnetization hysteresis loop with magnetic field along two opposite directions up to 1000 Oe at various temperatures from 1.8 to 7 K in the superconducting state. The diamond-like shape of the magnetization hysteresis loop indicates that this sample is a typical type-II superconductor.

The H_{c1} values at these selected temperatures are summarized in Figure 1e. The inset shows the method to determine H_{c1} based on the deviation of the linear behavior at higher field. The zero-temperature extrapolated value of $H_{c1}(0)$ is 261 ± 9.6 Oe by means of calculating the empirical law $H_{c1}(T)/H_{c1}(0) = 1 - (T/T_c)^2$. Figure 1f shows the H_{c2} versus T_c curve, and the T_c at applied filed is determined from the intercept of linear extrapolations from below and above the transition, as shown in the inset. The calculated $H_{c2}(0)$ at zero temperature is 978 ± 7.5 Oe by using the Werthamer−Helfand−Hohenberg (WHH) formula[30] $H_{c2}(0) = 0.693\text{-}[-dH_{c2}(T)/dT]_{T_c} \times T_c$, and 1092 ± 39 Oe by fitting $H_{c2}(T)$ with the expression $H_{c2}(T) = H_{c2}(0)[1 - (T/T_c)^2]/[1 + (T/T_c)^2]$ based on the Gonzburg−Landau theory.

Sample no. 50 was uncomplicatedly synthesized by just pestling the mixture of K metal and $C_{24}H_{18}$ with a mole ratio of 4:1 without annealing. As shown in Figure 2, the magnetization measurements provide evidence of the existence of superconductivity in this sample. Figure 2a represents the temperature dependence of the χ in the applied magnetic

DOI: 10.1021/acs.jpclett.8b03263
J. Phys. Chem. Lett. 2019, 10, 40−47

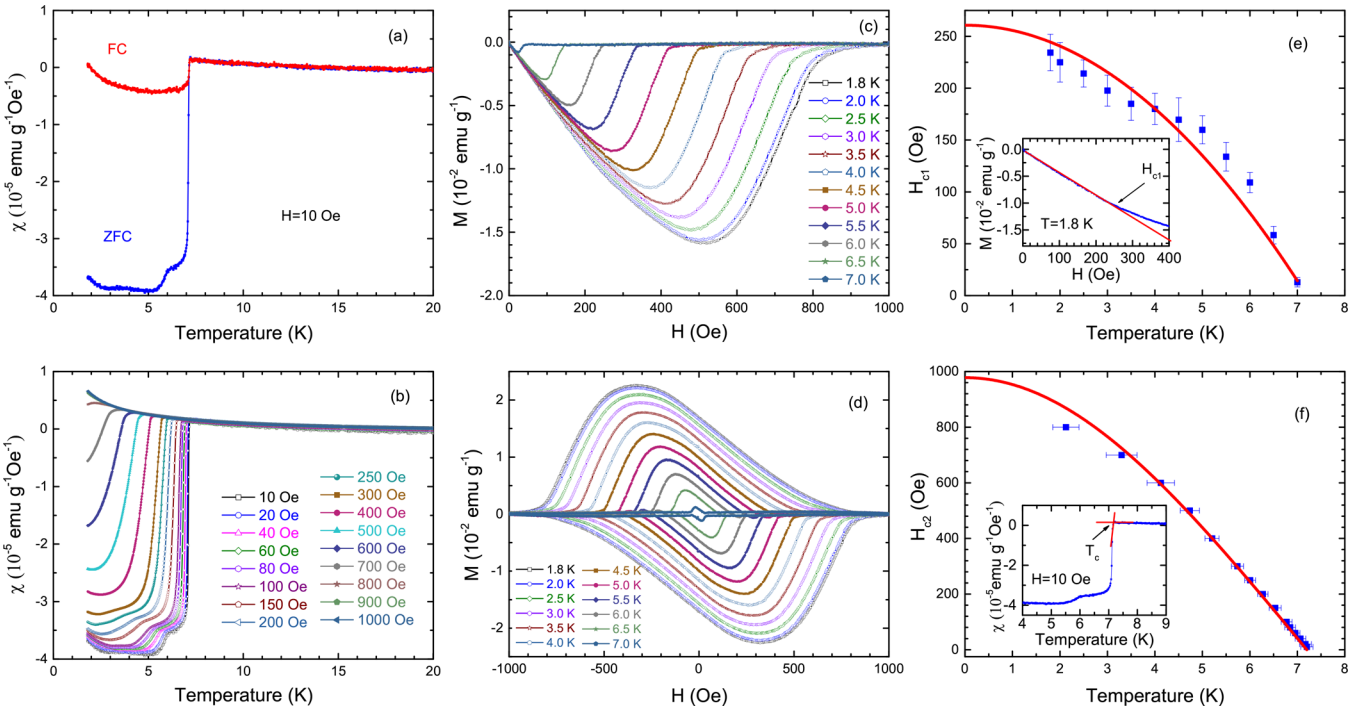

Figure 1. (a) Temperature dependence of the magnetic susceptibility χ for $K_xC_{24}H_{18}$ (sample no. 16) in the applied magnetic field of 10 Oe with field-cooling (FC) and zero-field cooling (ZFC). (b) Temperature dependence of the χ for $K_xC_{24}H_{18}$ measured at various magnetic fields up to 1000 Oe in the ZFC run. (c) Magnetic field dependence of the magnetization for $K_xC_{24}H_{18}$ at various temperatures in the superconducting state. (d) Magnetization hysteresis loop with scanning magnetic field along two opposite directions up to 1000 Oe measured at various temperatures in the superconducting state. (e) Temperature dependence of the lower critical field $H_{c1}(T)$. The error bars represent estimated uncertainty in determining H_{c1}. The inset shows the magnetic field dependence of the magnetization at the temperature of 1.8 K and the method for the determination of H_{c1}. (f) Temperature dependence of the upper critical field $H_{c2}(T)$. The error bars represent the uncertainty in the rounding of the transition. The inset shows that T_c is defined on the curve of the temperature dependence of the magnetic susceptibility in the applied magnetic field of 10 Oe with the ZFC run.

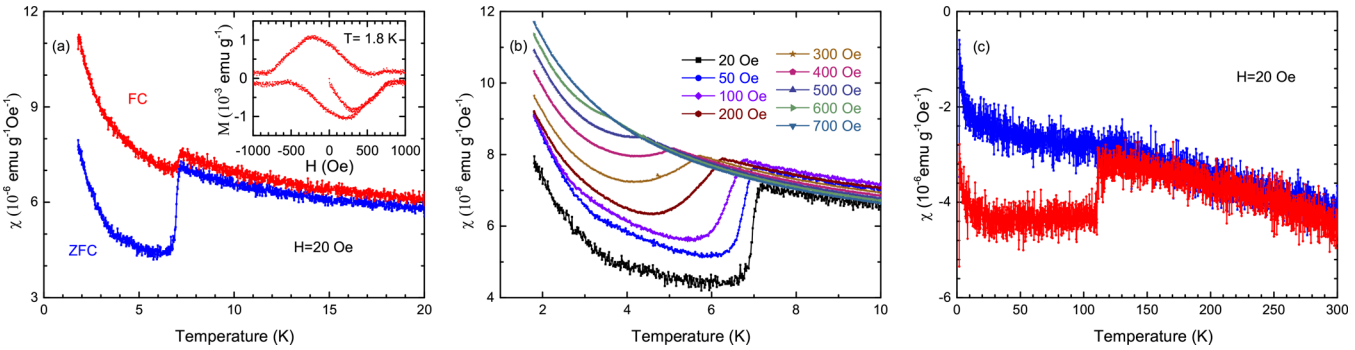

Figure 2. (a) Temperature dependence of the magnetic susceptibility χ for $K_xC_{24}H_{18}$ (sample no. 50) in the applied magnetic field of 10 Oe with the FC and ZFC runs. The inset shows the magnetization hysteresis loop with scanning magnetic field along two opposite directions up to 1000 Oe at the temperature of 1.8 K. (b) Temperature dependence of the magnetic susceptibility of $K_xC_{24}H_{18}$ (sample no. 50) measured at various magnetic fields up to 700 Oe in the FC run. (c) Temperature dependence of the magnetic susceptibility χ for $K_xC_{24}H_{18}$ (sample no. 10) in the applied magnetic field of 20 Oe with the FC and ZFC runs.

field of 20 Oe with the FC and ZFC runs. The ZFC curve shows a sudden decrease at the temperature of 7.2 K, and a small upturn after the drop can be seen in the FC run. There is an obvious paramagnetic background accompanying the superconducting phase. The inset of Figure 2a shows the magnetization hysteresis loop with magnetic field along two opposite directions up to 1000 Oe at 1.8 K after removal of the paramagnetic background. The shape of this loop is a typical characteristic for a superconductor. Figure 2b represents the temperature dependence of the χ measured at different magnetic fields up to 700 Oe in the ZFC processes. The superconducting fraction is suppressed by the applied magnetic fields. When the field is higher than 700 Oe, the superconducting transition is hardly observed. These features reveal that sample no. 50 is a new superconductor that is synthesized by just pestling without annealing.

In addition, a weak superconducting phase with a high T_c of 120 K was observed in sample no. 10, which was synthesized by pestling the mixture of K metal and $C_{24}H_{18}$ with a mole ratio of 3:1 without annealing. Figure 2c displays the temperature dependence of the χ for sample no. 10 in the applied magnetic field of 20 Oe with the FC and ZFC

DOI: 10.1021/acs.jpclett.8b03263
J. Phys. Chem. Lett. 2019, 10, 40−47

processes. The χ versus T curve exhibits a clear drop at the temperature of 120 K in the ZFC run, while the drop is too weak to be observed precisely in the FC run. This result supports the discovery of superconductivity in potassium-doped *p*-terphenyl with T_c of 123 K.[12] The superconducting phase with 120 K may be the common feature in *p*-oligophenyls with single C−C connected bond(s), but it is a weak superconducting phase.

The Meissner effect and zero resistivity are two fundamental features of superconductivity. However, the measurement of resistance is difficult in the metal-doped carbon-based superconductors because of the low volume fraction of superconducting content. Actually the metal-doped aromatic hydrocarbon superconductors were mainly detected from magnetic measurement.[31−35] However, herein we have succeeded in observing temperature dependence on resistance for the sample pressured at 4.7 GPa. The measured results are shown in Figure S1. We can see the visible drop of resistance with decreasing the temperature for both cooling and warming processes, though the zero resistance has not yet been realized. The result implies the possibility of high-T_c superconductivity in $K_xC_{24}H_{18}$.

To understand the superconductivity of $K_xC_{24}H_{18}$, we have investigated the Raman characteristics. Figure 3 shows the

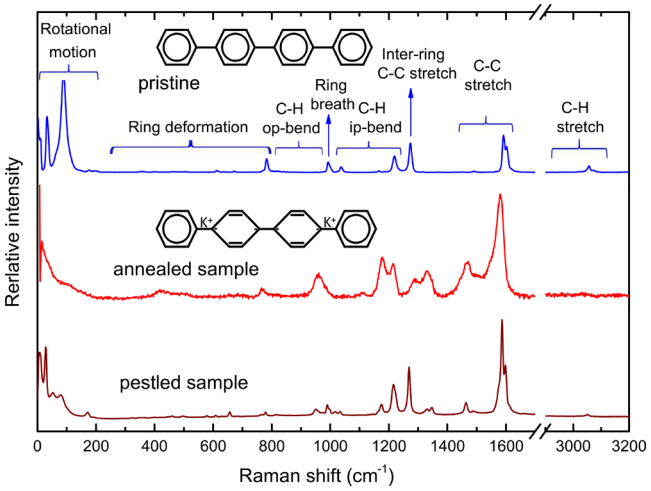

Figure 3. Room-temperature Raman scattering spectra of pristine sample (blue line), annealed sample (red line), and pestled sample (brown line). The sticks in the upper horizontal axis give the peak positions of the vibrational modes in the pristine sample.

Raman scattering spectra of the pristine, annealed, and pestled samples. The sticks over the pristine sample give the clarifications of the vibrational modes of the pristine $C_{24}H_{18}$.[36] The Raman spectra of the annealed sample can be duplicated in most annealed samples. This Raman spectrum in the red line implies the formation of bipolarons, and this scenario is consistent with previous works.[37] According to the theory of bipolarons, K atoms are intercalated into the C−C bonds between adjacent rings upon doping. Along the chain, the C−C bonds between rings are reduced. In the inner-rings, the parallel bonds decrease, whereas the inclined bonds increase. As a result, the inner-rings become quinoid. The molecule becomes a nearly coplanar conformation and forms the conjugate conformation in the chain, and it leads to high intrachain mobilities of charge carriers such as bipolarons.[38] In contrast with the Raman spectra of pristine and annealed sample, the following five aspects reveal the formation of bipolarons: First, the bipolaronic bands centered at 1581 cm^{-1} appear after the merging of the strong bands at 1591 and 1601 cm^{-1}. They show downshifts in wavenumber due to the increase of the inclined C−C bond lengths within the rings.[37] Second, the new bipolaronic band at 1470 cm^{-1} is associated with the vibrational mode of the C−H bond of external rings.[37] Third, the 1290 and 1332 cm^{-1} bands in the annealed sample originate from the inter-ring C−C stretching mode at the 1274 cm^{-1} band of the pristine sample. The upshifts in wavenumber reflect the decrease of length in the C−C bonds between rings. Fourthly, the two bipolaronic bands at 1179 and 1215 cm^{-1} correspond to the 1218 cm^{-1} band in the pristine. Finally, the new bipolarnic band at 961 cm^{-1} arises from the in-plane ring bend. Furthermore, in the pestled sample, the coexistence of the pristine and bipolarons can be obviously seen. Nevertheless, the intensity of the phonon modes in the pristine sample is stronger than that of bipolarons. The strong bands at around 1600 cm^{-1} are the overlap with the pristine and the bipolaron. The new band at 1465 cm^{-1} in the pestled sample is homologous to the band at 1470 cm^{-1} in the annealed sample. The band at 1274 cm^{-1} in the pristine sample evolves into bipolaronic bands at 1330 and 1347 cm^{-1} in the pestled sample, and the 1274 cm^{-1} band remains in the pestled sample as the component of the pristine sample. The 1174 cm^{-1} band in the pestled sample arises from the 1218 cm^{-1} band in the pristine sample. Moreover, in the pestled sample, parts of the bipolaronic bands are overlapped by the signal of the pristine sample. Admittedly, the Raman spectra provide evidence for the formation of bipolarons in both pestled and annealed samples.

The structural and electronic properties are valuable for understanding the obtained superconductivity. Hence, we analyzed the crystal and electronic structures of $K_xC_{24}H_{18}$ with the help of the first-principles simulation (more computational details can be found in the Supporting Information), which has been proved to be feasible for predicting the crystal structure

Table 2. Optimized Crystal Lattice Constants *a*, *b*, and *c*; the Angles *α*, *β*, and *γ* between Two Axes; and the Volume of Unit Cell (*V*) for Every Doping Level

compound	space group	*a* (Å)	*b* (Å)	*c* (Å)	*α* (deg)	*β* (deg)	*γ* (deg)	*V* (Å^3)
$C_{24}H_{18}$[a]	$P2_1/c$	18.899	5.61	8.11	90	109.47	90	810.68
$C_{24}H_{18}$	$P2_1/c$	18.744	5.532	7.906	90	108.64	90	776.8
$K_1C_{24}H_{18}$	$P1$	7.238	6.944	17.316	89.86	86.06	89.81	868.3
$K_2C_{24}H_{18}$	$P1$	6.910	5.910	17.710	90	99.83	90	712.7
$K_2C_{24}H_{18}$	$P2_1/c$	20.130	5.810	7.710	90	113.54	90	827.2
$K_3C_{24}H_{18}$	$P2_1$	20.783	7.097	7.257	90	119.51	90	931.6

[a]ref 41.

DOI: 10.1021/acs.jpclett.8b03263
J. Phys. Chem. Lett. 2019, 10, 40−47

of aromatic hydrocarbons.[14,15,39,40] For several possible K-doping levels x = 1, 2, and 3 in $K_xC_{24}H_{18}$, we carried out the random structure search and chose those structures satisfying the two requirements of having a relatively low formation energy and fitting the experimental XRD well. The crystal parameters of these satisfied structures are summarized in Table 2. Figure 4 shows the formation energy of $K_xC_{24}H_{18}$ (x = 1, 2, and 3) as a function of the K chemical potential. μ_K is the chemical potential of the K species, and μ_K(bulk) can be obtained from the energy per K atom in the K metal with the body-centered cubic structure. Here, $\mu_K = \mu_K$(bulk) means that the element is so rich that the pure element phase can form. $E_f < 0$ indicates that the doped compound is stable. As shown in Figure 4, the doping level of x = 2 results in the lower formation energy in the effective range of K chemical potential, which means that the $K_2C_{24}H_{18}$ phase is easy to obtain in experiments. For pristine $C_{24}H_{18}$, as shown in Table 2, we obtained the lattice constants according to the previous experiments.[41] In Figure 5a, the difference of several XRD peaks between our experiments and simulation mainly comes from the strong orientation along the (001) direction in our pristine sample. When the doping level is x = 1, namely $K_1C_{24}H_{18}$, the system transforms to $P1$ space group from $P2_1/c$. As shown in Figure S2, the quaterphenyl molecules exhibit the herringbone arrangement. However, by calculating the total energies at different magnetic states, we found that $K_1C_{24}H_{18}$ is stabilized at the antiferromagnetic state with 19.3 meV lower energy than the paramagnetic state. The phenomenon of the x = 1 doping level leading to antiferromagnetic ground state was also observed in K-doped biphenyl and p-terphenyl.[42] These results indicate that the observed superconducting phases are not in the composition of $K_1C_{24}H_{18}$.

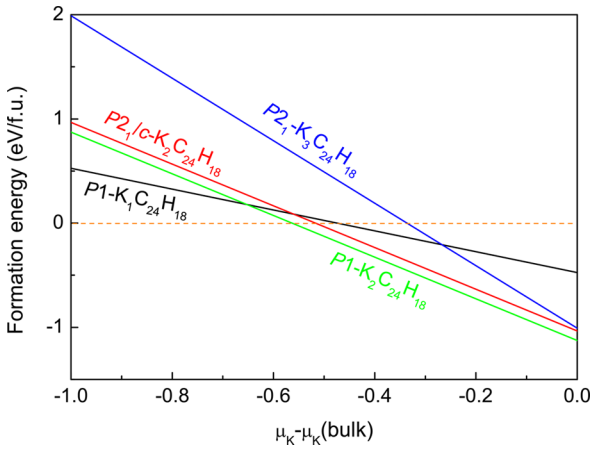

Figure 4. Calculated formation energy of $K_xC_{24}H_{18}$ as a function of the K chemical potential.

Increasing the K doping content to x = 2, namely, $K_2C_{24}H_{18}$, we obtained two structures with $P1$ and $P2_1/c$ space groups. Based on these two structures, the XRD spectra were calculated and compared with the experimental data for the samples with superconductivity at 7.2 K. As shown in panels b and c of Figure 5, the predicted $P1$-$K_2C_{24}H_{18}$ and $P2_1/c$-$K_2C_{24}H_{18}$ can reproduce the XRD patterns well for the annealed and pestled samples, respectively. Therefore, the annealed and pestled samples could have $P1$-$K_2C_{24}H_{18}$ and $P2_1/c$-$K_2C_{24}H_{18}$ structure, respectively. In the annealed sample,

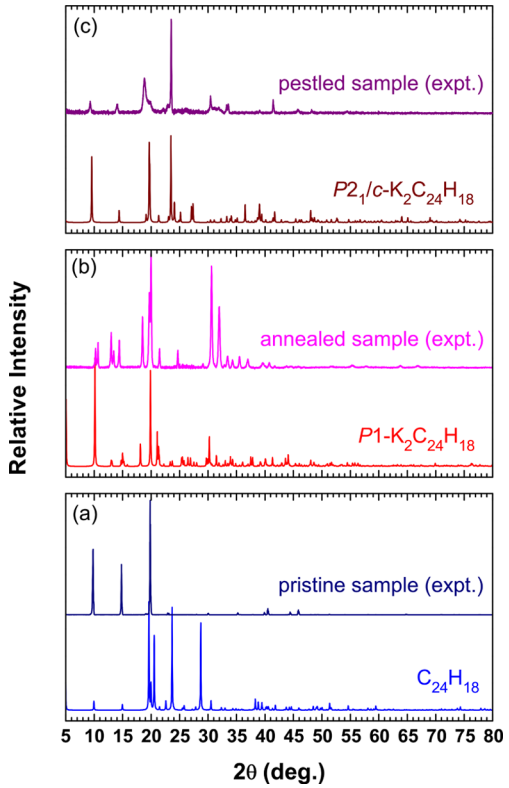

Figure 5. Calculated XRD spectra of $C_{24}H_{18}$ (a), $P1$-$K_2C_{24}H_{18}$ (b), and $P2_1/c$-$K_2C_{24}H_{18}$ (c) compared with the experimental ones. The experimental XRD patterns were taken from the pristine and K-doped samples (the annealed and pestled samples with T_c = 7.2 K). All XRD data were collected by using the incident wavelength λ = 1.5406 Å.

the low symmetry accounts for the complexity of its XRD peaks, such as double peaks around 14° and triple peaks around 20°. In contrast, the symmetry of $P2_1/c$ remained in the pestled sample, which makes their XRD peaks keep the partial characteristics of the pristine sample, such as the XRD peaks near 10° and 15°. The XRD analysis mirrors the Raman spectra shown above. Figure 6 shows the corresponding crystal structures. In comparison with pristine $C_{24}H_{18}$, the $P2_1/c$ symmetry is broken in the annealed sample ($P1$-$K_2C_{24}H_{18}$), but the herringbone structural feature remains, as shown in Figure 6b. Viewing along the a-direction, two K atoms respectively distribute on the C−C bonds connecting two benzene rings at the end of the molecule. The pestled sample ($P2_1/c$-$K_2C_{24}H_{18}$) keeps the $P2_1/c$ symmetry where two K atoms also distribute on the C−C bonds connecting two benzene rings at the end of the molecule viewed along the c-direction. However, as shown in Figure 6c, $P2_1/c$-$K_2C_{24}H_{18}$ exhibits a clear layered structure viewing along the b-direction. Figure 6 displays the visible difference among pristine, annealed, and pestled samples. (More structure information on doped systems, including atomic positions, can be found in the Supporting Information.)

For the doping level up to x = 3, namely, $K_3C_{24}H_{18}$, the crystal structure shown in Figure S3 exhibits the herringbone feature with $P2_1$ space group. However, there is big deviation of XRD peaks between $P2_1$-$K_3C_{24}H_{18}$ and annealed/pestled sample with T_c = 7.2 K (as seen from Figures 5 and S4). This indicates that the low-T_c phase should not be a result of the three-electron doping. Similar to K-doped biphenyl and p-terphenyl,[42] $K_xC_{24}H_{18}$ with high doping levels such as x = 2

DOI: 10.1021/acs.jpclett.8b03263
J. Phys. Chem. Lett. 2019, 10, 40−47

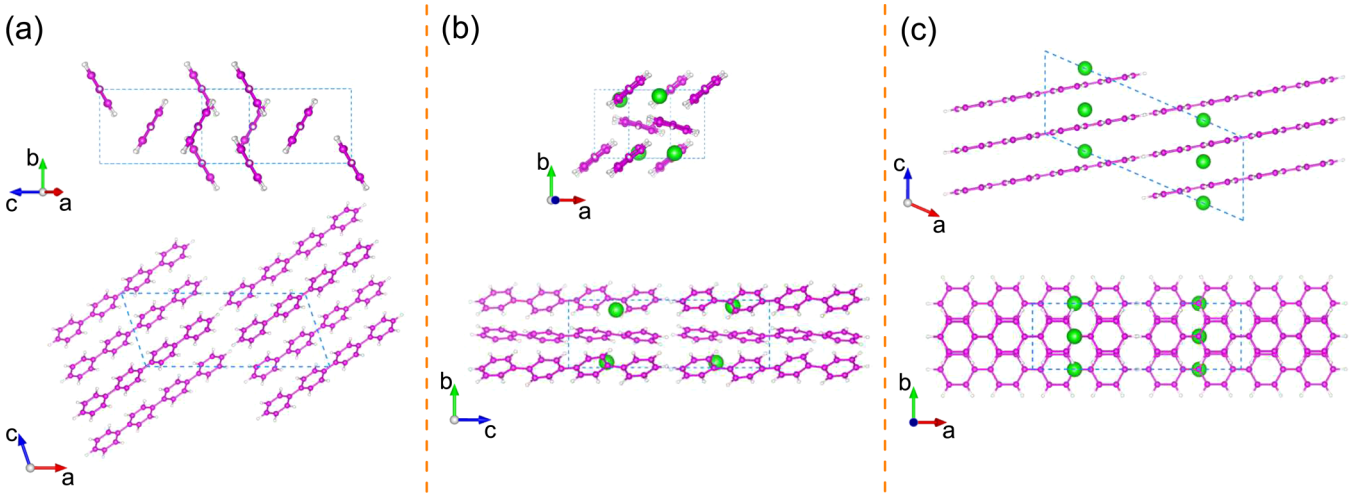

Figure 6. Optimized structures of $C_{24}H_{18}$ (a), $P1$-$K_2C_{24}H_{18}$ (b), and $P2_1/c$-$K_2C_{24}H_{18}$ (c) viewing from different directions. Pink, white, and green balls represent C, H, and K atoms, respectively. Dashed blue line marks the size of the unit cell.

and $x = 3$ was predicted to exhibit the nonmagnetic feature. From this viewpoint, $K_xC_{24}H_{18}$ with the high doping concentration could be a potential superconductor.

Focusing on $P1$-$K_2C_{24}H_{18}$ and $P2_1/c$-$K_2C_{24}H_{18}$, we have also calculated their electronic structures to further understand the observed superconductivity. The intercalation of K atoms into the pristine sample brings about the charge transfer, as shown in Figure 7. The charge transferred from K atoms to organic molecules mainly distributes on the C−C bridge bonds and those C atoms near them, which looks like bipolaronic characteristics. Noticeably, $P1$-$K_2C_{24}H_{18}$ is a semiconductor with a small band gap of 0.1 eV, lacking the metallicity (Figure S5). However, similar to other hydrocarbons,[15,40] a small charge fluctuation, such as ±0.1e, will make $P1$-$K_2C_{24}H_{18}$ behave like a metal. For examples, the ±0.1e in $P1$-$K_2C_{24}H_{18}$ can result in the electronic density of state at the Fermi level (N_{E_F}) reaching 2.61 and 3.75 states/eV/f.u., respectively. The N_{E_F} of $P1$-$K_2C_{24}H_{18}$ with the charge fluctuations is similar to that of K_2biphenyl,[15] and slightly less than those of K_2benzene,[13] K_3picene,[43] K_2phenanthrene,[44] and $K_{2.5}$terphenyl.[14] However, the N_{E_F} can be tuned by changing the doping content around $x \approx 2$ for $K_{2+\delta}C_{18}H_{14}$ ($0 < \delta < 1$). $P2_1/c$-$K_2C_{24}H_{18}$, corresponding to the pestled sample, itself is a metal with the N_{E_F} of 4.5 states/eV/f.u., which is in agreement with those of K_2benzene,[13] K_3picene,[43] K_2phenanthrene,[44] and $K_{2.5}$terphenyl.[14] Four bands cross the Fermi level in $P2_1/c$-$K_2C_{24}H_{18}$ (Figure S6), showing the complicated feature of the band structure. On the basis of the comparable N_{E_F} of $P2_1/c$-$K_2C_{24}H_{18}$ with K-doped benzene, picene, phenanthrene, and *p*-terphenyl, in the range of 4−6 states/eV/f.u., and combined with the similar feasible screened Coulomb pseudopotential μ^* of 0.1, we can predict that the T_c of $P2_1/c$-$K_2C_{24}H_{18}$ is in the range of 5−8 K, which is in accordance with our experimental observation. Using the same approach, the T_c of $P1$-$K_2C_{24}H_{18}$ with ±0.1e is predicted as slightly less than that of $P2_1/c$-$K_2C_{24}H_{18}$. As a result, the low electronic densities of states at the Fermi level correspond to the low-T_c superconducting phase.[13−15,39,40] The high-T_c superconductivity observed in sample no. 10 is suggested to result from the higher doping concentration, such as the doping with three electrons. This is because we have observed higher density of states at Fermi level in $P2_1$-$K_3C_{24}H_{18}$ (Figure S7). Only the high doping content will reduce the stability of the system.

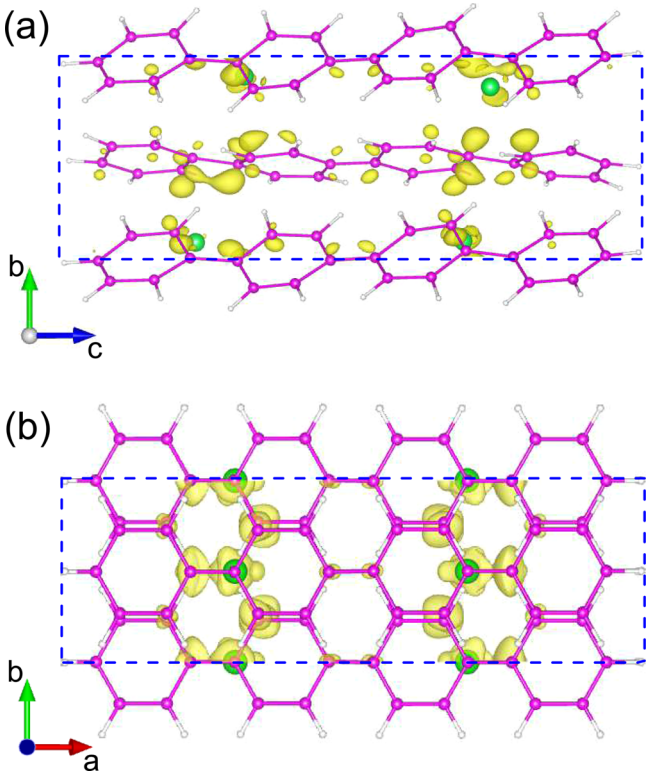

Figure 7. Calculated 3D plots of different charge density for $P1$-$K_2C_{24}H_{18}$ (a) and $P2_1/c$-$K_2C_{24}H_{18}$ (b) with the isosurface unit of 3×10^{-3} e/a.u.^{3} Pink, white, and green balls represent C, H, and K atoms, respectively. The yellow areas indicate the increase of electrons in this region, namely the charge transferred from K atom to molecules. The dashed blue line marks the size of the unit cell.

In summary, encouraged by the discovery of superconductivity in potassium-doped *p*-terphenyl, we have examined such a possibility in *p*-quaterphenyl with one more phenyl ring than *p*-terphenyl based on the consideration that the conductivity increases with increasing chain length in the poly-*p*-phenylene family. The samples were synthesized in

DOI: 10.1021/acs.jpclett.8b03263
J. Phys. Chem. Lett. 2019, 10, 40−47

various conditions of annealing or just pestling. The Meissner effect with critical temperatures ranging from 3.5 to 120 K is observed by the magnetic susceptibility measurements. The superconducting phase of 7.2 K can be duplicated in several samples with superconductivity and seems to be the most stable phase. In comparison with previous reports about superconductivity in K-doped *p*-terphenyl, biphenyl, *p*-quinquephenyl, and 2,2′-bipyridine, the primary 7.2 K superconducting phase may be the common character in chain linking molecules, corresponding to the two-electron doping. Analogously, the weak 120 K superconducting phase in K-doped *p*-quaterphenyl is probably due to the higher doping concentration. This is similar to the superconducting phase with T_c above 120 K in K-doped *p*-terphenyl. In both the annealed and pestled samples with superconductivity, the charge transfer from metal to molecule was confirmed from the Raman scattering measurements. The realization of superconductivity in potassium-doped *p*-quaterphenyl supports the discovery of superconductivity in potassium-doped *p*-terphenyl and adds a new league of superconductors in the *p*-oligophenyl family. The innovation of a synthetic method using just pestling without annealing opens up a new avenue for the synthesis of organic superconductors.

■ ASSOCIATED CONTENT

Supporting Information

The Supporting Information is available free of charge on the ACS Publications website at DOI: 10.1021/acs.jpclett.8b03263.

Synthesis and first-principles calculation methods, resistance measurement, predicted crystal structure, atomic positions, electronic density of states and band structures of K-doped *p*-quaterphenyl (PDF)

■ AUTHOR INFORMATION

Corresponding Authors

*E-mail: haiqing0@csrc.ac.cn. Phone: +86 10 56981818. Fax: +86 10 56981818.

*E-mail: xjchen@hpstar.ac.cn. Phone: +86 21 80177044. Fax: +86 21 80177064.

ORCID

Guo-Hua Zhong: 0000-0003-0673-8738

Kai Zhang: 0000-0001-9959-319X

Author Contributions

‖J.-F.Y. and G.-H.Z. contributed equally to this work

Notes

The authors declare no competing financial interest.

■ ACKNOWLEDGMENTS

Experiments were supported by the National Key R&D Program of China (Grant No. 2018YFA0305900). The calculations were supported by the National Natural Science Foundation of China (Grant Nos. 61574157 and 61774164), the Basic Research Program of Shenzhen (Grant Nos. JCYJ20170818153404696 and JCYJ20150925163313898), and NSAF U1530401. The partial calculations were supported by the Special Program for Applied Research on Super Computation of the NSFC-Guangdong Joint Fund (the second phase) under Grant No. U1501501.

■ REFERENCES

(1) Ginzburg, V. L. High-Temperature Superconductivity-Dream or Reality? *Sov. Phys. Usp.* **1976**, *19*, 174−179.

(2) Little, W. A. Possibility of Synthesizing an Organic Superconductor. *Phys. Rev.* **1964**, *134*, A1416−A1424.

(3) Heeger, A. J.; Kivelson, S.; Schrieffer, J. R.; Su, W. P. Solitons in Conducting Polymers. *Rev. Mod. Phys.* **1988**, *60*, 781.

(4) Shacklette, L. W.; Chance, R. R.; Ivory, D. M.; Miller, G. G.; Baughman, R. H. Electrical and Optical Properties of Highly Conducting Charge-Transfer Complexes of Poly (*p*-Phenylene). *Synth. Met.* **1980**, *1*, 307−320.

(5) Anderson, P. W. Model for the Rlectronic Structure of Amorphous Semiconductors. *Phys. Rev. Lett.* **1975**, *34*, 953−955.

(6) Kuivalainen, P.; Stubb, H.; Isotalo, H.; YliLahti, P.; Holmström, C. Electrical and Optical Properties of $FeCl_3$-Doped Polyparaphenylene $[(p\text{-}C_6H_4)_x]$. *Phys. Rev. B: Condens. Matter Mater. Phys.* **1985**, *31*, 7900.

(7) Ivory, D. M.; Miller, G. G.; Sowa, J. M.; Shacklette, L. W.; Chance, R. R.; Baughman, R. H. Highly Conducting Charge-Transfer Complexes of Poly(*p*-Phenylene). *J. Chem. Phys.* **1979**, *71*, 1506−1507.

(8) Havinga, E. E.; Van Horssen, L. W. Dependence of the Electrical Conductivity of Heavily-Doped Poly-*p*-Phenylenes on the Chain Length. *Synth. Met.* **1986**, *16*, 55−70.

(9) Brédas, J. L. Relationship between Band Gap and Bond Length Alternation in Organic Conjugated Polymers. *J. Chem. Phys.* **1985**, *82*, 3808−3811.

(10) Wang, R.-S.; Gao, Y.; Huang, Z.-B.; Chen, X.-J. Superconductivity in *p*-Terphenyl. 2017, arXiv:1703.05803. arXiv.org e-Print archive. http://arxiv.org/abs/1703.05803 (accessed Mar 16, 2017).

(11) Wang, R.-S.; Gao, Y.; Huang, Z.-B.; Chen, X.-J. Superconductivity at 43 K in a Single C-C Bond Linked Terphenyl. 2017, arXiv:1703.05804. arXiv.org e-Print archive. http://arxiv.org/abs/1703.05804 (accessed Mar 16, 2017).

(12) Wang, R.-S.; Gao, Y.; Huang, Z.-B.; Chen, X.-J. Superconductivity Above 120 K in a Chain Link Molecule. 2017, arXiv:1703.06641. arXiv.org e-Print archive. http://arxiv.org/abs/1703.06641 (accessed Mar 20, 2017).

(13) Zhong, G.; Chen, X.-J.; Lin, H.-Q. Prediction of Superconductivity in Potassium-Doped Benzene. 2015, arXiv:1501.00240. arXiv.org e-Print archive. http://arxiv.org/abs/1501.00240 (accessed Jan 1, 2015).

(14) Zhong, G.-H.; Wang, X.-H.; Wang, R.-S.; Han, J.-X.; Zhang, C.; Chen, X.-J.; Lin, H.-Q. Structural and Bonding Characteristics of Potassium-Doped *p*-Terphenyl Superconductors. *J. Phys. Chem. C* **2018**, *122*, 3801−3808.

(15) Zhong, G.-H.; Yang, D.-Y.; Zhang, K.; Wang, R.-S.; Zhang, C.; Lin, H.-Q.; Chen, X.-J. Superconductivity and Phase Stability of Potassium-Doped Biphenyl. *Phys. Chem. Chem. Phys.* **2018**, *20*, 25217−25223.

(16) Huang, G.; Wang, R.-S.; Chen, X.-J. Observation of Meissner Effect in Potassium-Doped *p*-Quinquephenyl. 2018, arXiv:1801.06324. arXiv.org e-Print archive. http://arxiv.org/abs/1801.06324 (accessed Jan 24, 2018).

(17) Zhang, K.; Wang, R.-S.; Qin, A.-J.; Chen, X.-J. Superconductivity in Potassium-Doped 2,2′-Bipyridine. 2018, arXiv:1801.06320. arXiv.org e-Print archive. http://arxiv.org/abs/1801.06320 (accessed Jan 24, 2018).

(18) Wang, R.-S.; Cheng, J.; Wu, X.-L.; Yang, H.; Chen, X.-J.; Gao, Y.; Huang, Z.-B. Superconductivity at 3.5 K and/or 7.2 K in Potassium-Doped Triphenylbismuth. *J. Chem. Phys.* **2018**, *149*, 144502.

(19) Li, H.; Zhou, X.; Parham, S.; Nummy, T.; Griffith, J.; Gordon, K.; Chronister, E. L.; Dessau, D. S. Spectroscopic Evidence of Low Energy Gaps Persisting Towards 120 K in Surface-Doped *p*-Terphenyl Crystals. 2018, arXiv:1704.04230. arXiv.org e-Print archive. http://arxiv.org/abs/1704.04230 (accessed Mar 29, 2018).

DOI: 10.1021/acs.jpclett.8b03263
J. Phys. Chem. Lett. 2019, 10, 40−47

(20) Ren, M. Q.; Chen, W.; Liu, Q.; Chen, C.; Qiao, Y. J.; Chen, Y. J.; Zhou, G.; Zhang, T.; Yan, Y. J.; Feng, D. L. Observation of Novel Gapped Phases in Potassium Doped Single Layer *p*-Terphenyl on Au (111). 2017, arXiv:1705.09901. arXiv.org e-Print archive. http://arxiv.org/abs/1705.09901 (accessed May 28, 2017).
(21) Neha, P.; Sahu, V.; Patnaik, S. Facile Synthesis of Potassium Intercalated *p*-Terphenyl and Signatures of a Possible High T_c phase. 2017, arXiv:1712.01766. arXiv.org e-Print archive. http://arxiv.org/abs/1712.01766 (accessed Dec 5, 2017).
(22) Geilhufe, R. M.; Borysov, S. S.; Kalpakchi, D.; Balatsky, A. V. Towards Novel Organic High-T_c Superconductors: Data Mining using Density of States Similarity Search. 2018, arXiv:1709.03151. arXiv.org e-Print archive. http://arxiv.org/abs/1709.03151 (accessed Jan 22, 2018).
(23) Fabrizio, M.; Qin, T.; Naghavi, S. S.; Tosatti, E. Two-Band $S_{\pm}$ Strongly Correlated Superconductivity in K_3 p-Terphenyl? 2017, arXiv:1705.05066. arXiv.org e-Print archive. http://arxiv.org/abs/1705.05066 (accessed May 15, 2017).
(24) Mazziotti, M. V.; Valletta, A.; Campi, G.; Innocenti, D.; Perali, A.; Bianconi, A. Possible Fano Resonance for High T_c Multi-Gap Superconductivity in p-Terphenyl Doped by K at the Lifshitz Transition. 2017, arXiv:1705.09690. arXiv.org e-Print archive. http://arxiv.org/abs/1705.09690 (accessed May 26, 2017).
(25) Liu, W.; Lin, H.; Kang, R.; Zhu, X.; Zhang, Y.; Zheng, S.; Wen, H.-H. Magnetization of Potassium-Doped *p*-Terphenyl and *p*-Quaterphenyl by High Pressure Synthesis. *Phys. Rev. B: Condens. Matter Mater. Phys.* **2017**, *96*, 224501.
(26) Gundlach, D. J.; Lin, Y. Y.; Jackson, T. N.; Schlom, D. G. Oligophenyl-Based Organic Thin Film Transistors. *Appl. Phys. Lett.* **1997**, *71*, 3853−3855.
(27) Hosokawa, C.; Higashi, H.; Kusumoto, T. Novel Structure of Organic Electroluminescence Cells with Conjugated Oligomers. *Appl. Phys. Lett.* **1993**, *62*, 3238−3240.
(28) Quochi, F. Random Lasers Based on Organic Epitaxial Nanofibers. *J. Opt.* **2010**, *12*, 024003−24011.
(29) Leising, G.; Tasch, S.; Meghdadi, F.; Athouel, L.; Froyer, g.; Scherf, U. Blue Electroluminescence with Ladder-Type Poly(*para*-Phenylene) and *para*-Hexaphenyl. *Synth. Met.* **1996**, *81*, 185−189.
(30) Werthamer, N. R.; Helfand, E.; Hohenberg, P. C. Temperature and Purity Dependence of the Superconducting Critical Field, H_{c2}III. Electron Spin and Spin-Orbit Effects. *Phys. Rev.* **1966**, *147*, 295.
(31) Mitsuhashi, R.; Suzuki, Y.; Yamanari, Y.; Mitamura, H.; Kambe, T.; Ikeda, N.; Okamoto, H.; Fujiwara, A.; Yamaji, M.; Kawasaki, N.; Maniwa, Y.; Kubozono, Y. Superconductivity in Alkali-Metal-Doped Picene. *Nature* **2010**, *464*, 76−79.
(32) Wang, X. F.; Liu, R. H.; Gui, Z.; Xie, Y. L.; Yan, Y. J.; Ying, J. J.; Luo, X. G.; Chen, X. H. Superconductivity at 5 K in Alkali-Metal-Doped Phenanthrene. *Nat. Commun.* **2011**, *2*, 507−513.
(33) Kubozono, Y.; Mitamura, M.; Lee, X.; He, X.; Yamanari, Y.; Takahashi, Y.; Suzuki, Y.; Kaji, Y.; Eguchi, R.; Akaike, K.; Kambe, T.; Okamoto, H.; Fujiwara, A.; Kato, T.; Kosugi, T.; Aoki, H. Metal-Intercalated Aromatic Hydrocarbons: A New Class of Carbon-Based Superconductors. *Phys. Chem. Chem. Phys.* **2011**, *13*, 16476−16493.
(34) Artioli, G. A.; Hammerath, F.; Mozzati, M. C.; Carretta, P.; Corana, F.; Mannucci, B.; Margadonna, S.; Malavasi, L. Superconductivity in Sm-doped [*n*]Phenacenes (*n* = 3, 4, 5). *Chem. Commun.* **2015**, *51*, 1092−1095.
(35) Xue, M. Q.; Cao, T. B.; Wang, D. M.; Wu, Y.; Yang, H. X.; Dong, X. L.; He, J. B.; Li, F. W.; Chen, G. F. Superconductivity Above 30 K in Alkali-Metal Doped Hydrocarbon. *Sci. Rep.* **2012**, *2*, 389−392.
(36) Honda, K.; Furukawa, Y. Conformational Analysis of p-Terphenyl by Vibrational Spectroscopy and Density Functional Theory Calculations. *J. Mol. Struct.* **2005**, *735-736*, 11−19.
(37) Dubois, M.; Froyer, G.; Louarn, G.; Billaud, D. Raman Spectroelectrochemical Study of Sodium Intercalation into Poly(*p*-Phenylene). *Spectrochim. Acta, Part A* **2003**, *59*, 1849−1856.
(38) Brédas, J. L.; Street, G. B.; Thémans, B.; André, J. M. Organic Polymers Based on Aromatic Rings (Polyparaphenylene, Polypyrrole, Polythiophene): Evolution of the Electronic Properties as a Function of the Torsion Angle between Adjacent Rings. *J. Chem. Phys.* **1985**, *83*, 1323−1329.
(39) Zhong, G.-H.; Zhang, C.; Yan, X.; Li, X.; Du, Z.; Jing, G.; Ma, C. Structural and Electronic Properties of Potassium Doped 1,2;8,9-Dibenzopentacene Superconductor: Comparing with Doped [7]-Phenacenes. *Mol. Phys.* **2017**, *115*, 472−483.
(40) Wang, X.; Zhong, G.; Yan, X.; Chen, X.; Lin, H. First-Principles Prediction on Geometrical and Electronic Properties of K-Doped Chrysene. *J. Phys. Chem. Solids* **2017**, *104*, 56−61.
(41) Delugeard, Y.; Desuche, J.; Baudour, J. L. Structural transition in polyphenyls. II. The crystal structure of the high-temperature phase of quaterphenyl. *Acta Crystallogr., Sect. B: Struct. Crystallogr. Cryst. Chem.* **1976**, *32*, 702−705.
(42) Zhong, G.-H.; Zhang, C.; Chen, M.; Chen, X.-J.; Lin, H.-Q. Magnetic Transitions in K-Doped Biphenyl and *p*-Terphenyl. *IEEE Trans. Magn.* **2018**, *54*, 7002105.
(43) Casula, M.; Calandra, M.; Profeta, G.; Mauri, F. Intercalant and Intermolecular Phonon Assisted Superconductivity in K-Doped Picene. *Phys. Rev. Lett.* **2011**, *107*, 137006.
(44) Yan, X.-W.; Zhang, C. F.; Zhong, G. H.; Ma, D. W.; Gao, M. The Atomic Structures and Electronic Properties of Potassium-Doped Phenanthrene from a First-Principles Study. *J. Mater. Chem. C* **2016**, *4*, 11566.

DOI: 10.1021/acs.jpclett.8b03263
J. Phys. Chem. Lett. 2019, 10, 40−47